J Physiol 592.18 (2014) pp 4051–4068

The Journal of Physiology

Ano1, a Ca^{2+}-activated Cl^- channel, coordinates contractility in mouse intestine by Ca^{2+} transient coordination between interstitial cells of Cajal

Raman Deep Singh[1], Simon J. Gibbons[1], Siva Arumugam Saravanaperumal[1], Peng Du[2], Grant W. Hennig[3], Seth T. Eisenman[1], Amelia Mazzone[1], Yujiro Hayashi[1], Chike Cao[1], Gary J. Stoltz[1], Tamas Ordog[1], Jason R. Rock[4], Brian D. Harfe[5], Joseph H. Szurszewski[1] and Gianrico Farrugia[1]

[1]*Department of Physiology and Biomedical Engineering Enteric NeuroScience Program, Mayo Clinic, Rochester, MN, USA*
[2]*Auckland Bioengineering Institute, University of Auckland, Auckland, New Zealand*
[3]*Department of Physiology and Cell Biology, University of Nevada School of Medicine, Reno, NV, USA*
[4]*Department of Anatomy, UCSF School of Medicine, San Francisco, CA, USA*
[5]*Department of Molecular Genetics and Microbiology Genetics Institute, University of Florida, College of Medicine, Gainesville, FL, USA*

Key points

- Ano1, a Ca^{2+}-activated Cl^- channel, is expressed in interstitial cells of Cajal (ICC) throughout the gut. We report here that it is required to maintain coordinated Ca^{2+} transients within myenteric ICC of mouse small intestine. Ca^{2+} transients in Ano1 WT mice were rhythmic and coordinated whereas uncoordinated Ca^{2+} transients were seen in knockout mice.
- Ca^{2+} transients were un-coordinated following pharmacological block of Ano1 in WT mice using niflumic acid, 5-nitro-2-(3-phenylpropylamino) benzoic acid and 4,4′-diisothiocyanato-2,2′-stilbenedisulfonic acid disodium salt. Transient knockdown of Ano1 in organotypic cultures with short hairpin RNA to Ano1 in WT tissues also caused loss of coordinated Ca^{2+} transients.
- Contractility of Ano1 knockout mouse intestinal segments in organ bath experiments was significantly decreased, less coordinated and non-rhythmic. Spatiotemporal maps from knockout mouse small intestine also showed loss of phasic contractile activity.
- This study provides important information on the basic mechanisms driving coordinated contractile activity in the gastrointestinal tract.

Abstract Interstitial cells of Cajal (ICC) are pacemaker cells that generate electrical activity to drive contractility in the gastrointestinal tract via ion channels. Ano1 (*Tmem16a*), a Ca^{2+}-activated Cl^- channel, is an ion channel expressed in ICC. Genetic deletion of Ano1 in mice resulted in loss of slow waves in smooth muscle of small intestine. In this study, we show that Ano1 is required to maintain coordinated Ca^{2+} transients between myenteric ICC (ICC-MY) of small intestine. First, we found spontaneous Ca^{2+} transients in ICC-MY in both Ano1 WT and knockout (KO) mice. However, Ca^{2+} transients within the ICC-MY network in Ano1 KO mice were uncoordinated, while ICC-MY Ca^{2+} transients in Ano1 WT mice were rhythmic and coordinated. To confirm the role of Ano1 in the loss of Ca^{2+} transient coordination, we used pharmacological inhibitors of Ano1 activity and shRNA-mediated knock down of Ano1 expression in organotypic cultures of Ano1 WT small intestine. Coordinated Ca^{2+} transients became uncoordinated using both these approaches, supporting the conclusion that Ano1 is required to maintain coordination/rhythmicity of Ca^{2+} transients. We next determined the effect on smooth muscle contractility using spatiotemporal maps of contractile activity in Ano1 KO and WT tissues. Significantly decreased contractility that appeared to be non-rhythmic

DOI: 10.1113/jphysiol.2014.277152

and uncoordinated was observed in Ano1 KO jejunum. In conclusion, Ano1 has a previously unidentified role in the regulation of coordinated gastrointestinal smooth muscle function through coordination of Ca^{2+} transients in ICC-MY.

(Received 16 May 2014; accepted after revision 12 July 2014; first published online 25 July 2014)
Corresponding Author Gianrico Farrugia; Enteric NeuroScience Program, Mayo Clinic, 200 1st Street SW, Rochester, MN 55905, USA. Email: farrugia.gianrico@mayo.edu

Abbreviations Ano, anoctamin; CFTR, cystic fibrosis transmembrane conductance regulator; C_t, threshold cycle number; DIDS, 4,4′-diisothiocyanato-2,2′-stilbenedisulphonic acid disodium salt; ICC, interstitial cells of Cajal; ICC-MY, interstitial cells of Cajal at the level of the myenteric plexus; KO, knockout; KRB, Krebs–Ringer buffer; MOI, multiplicity of infection; NFA, niflumic acid; NPPB, 5-nitro-2-(3-phenylpropylamino) benzoic acid; NT, non-targeting; PND, postnatal day; qRT-PCR, quantitative RT-PCR; ROI, regions of interest; shRNA, short hairpin RNA.

Introduction

Ca^{2+}-activated Cl^- channels are present in nearly every cell type, fulfiling diverse functions. The identity of the Ca^{2+}-activated Cl^- channel involved in regulation of vascular tone and fluid secretion was unclear until the identification of Ano1 (TMEM16A, anoctamin1) as a gene that encoded a Ca^{2+}-activated, outwardly rectifying Cl^- selective ion channel when expressed in heterologous systems (Berg *et al.* 2012). Ano1 gating is both Ca^{2+}- and voltage-dependent. Ano1 is part of a 10-member family of anoctamins (ANion selective with eight OCT transmembrane segments), some members of which contribute to Ca^{2+}-activated Cl^- channel currents in various cell types (Schreiber *et al.* 2010). Several of these, but particularly Ano1, 2, 5 and 6 have been studied in detail (Schroeder *et al.* 2008, Stephan *et al.* 2009, Sagheddu *et al.* 2010, Martins *et al.* 2011, Tran *et al.* 2014). Ano4–10 when expressed in HEK293 cells produce transient Ca^{2+}-activated Cl^- currents using whole cell patch clamping albeit with lower current density than Ano1 (Tian *et al.* 2012). Ano6, also known as TMEM16F, has been also reported to function as a non-selective cation channel and lipid scramblase (Yang *et al.* 2012).

The exact role Ano1 plays in regulation of cell activity varies according to cell type. In lung and gastrointestinal tract epithelial cells, Ano1, together with the cystic fibrosis transmembrane conductance regulator (CFTR) Cl^- channel, contributes to the regulation of secretion (Kunzelmann *et al.* 2012). In arterial and tracheal smooth muscle cells opening of Ca^{2+}-activated Cl^- channels, probably Ano1 channels, depolarizes the membrane potential contributing to Ca^{2+} entry through Ca^{2+} channels and leading to contraction (Bulley & Jaggar, 2013). In the gastrointestinal muscle layers Ano1 is expressed not in smooth muscle, but in a specialized cell type referred to as the interstitial cells of Cajal (ICC) (Gomez-Pinilla *et al.* 2009). ICC generate a cyclic oscillation in membrane potential that regulates the smooth muscle membrane potential (slow wave) with contractions occurring at the peak of the depolarization (Thuneberg, 1982, Szurszewski, 1987, Huizinga *et al.* 1995, Torihashi *et al.* 1995, Ward *et al.* 1994). ICC also regulate the resting gastrointestinal smooth muscle cell membrane potential (Farrugia *et al.* 2003). Therefore, ICC act as gastrointestinal pacemaker cells together with other roles that include neuromodulation and mechanotransduction (Ward *et al.* 2000, Ward & Sanders, 2006, Kraichely & Farrugia, 2007).

To digest food, absorb nutrient and eliminate waste, gastrointestinal smooth muscle contractile activity needs to be coordinated. Ano1 knockout (KO) mice lack a smooth muscle slow wave and have irregular contractile activity (Hwang *et al.* 2009). However, the exact mechanism by which the Cl^- channel Ano1 results in coordinated smooth muscle function is not known. Calcium is an important signalling molecule both within and outside the gastrointestinal tract. Calcium regulation involves multiple feedback loops including from membrane ion channels. ICC at the level of the myenteric plexus of the small intestine (ICC-MY) (Rich *et al.* 2002, Torihashi *et al.* 2002, Yamazawa & Iino, 2002) display Ca^{2+} transients which activate and coordinate smooth muscle contractions (Park *et al.* 2006). The aim of this study was therefore to determine if Ano1 is required to coordinate ICC Ca^{2+} transients and subsequent coordinated smooth muscle contractile activity. We found that loss of Ano1 activity results in uncoordinated Ca^{2+} transients in ICC, resulting in loss of coordinated smooth muscle contractility and suggesting a new role for Ano1 in the regulation of coordinated gastrointestinal smooth muscle function.

Methods

Animals

Ano1 KO mice were obtained by breeding mice heterozygous for a targeted disruption of the Ano1 gene (Rock *et al.* 2008). Ano1 KO mice were confirmed by phenotype and PCR-based genotyping (Stanich *et al.*

2011). Postnatal day (PND) 10–21 mice were killed by carbon dioxide inhalation and jejunum was dissected and placed in oxygenated Krebs–Ringer buffer (KRB) until further use. The mice used in this study were maintained and the experiments were done with approval from the Institutional Animal Care and Use Committee of the Mayo Clinic.

Tissue preparation

The whole muscle tissue preparation from jejunum was prepared as follows. A small jejunal segment, about 15 mm in length, was cut and placed into a 60 mm dish coated with Sylgard elastomer (Dow Corning Corp., Midland, MI, USA) and filled with KRB. The tube was then cut along the mesenteric border and pinned out flat with the serosa facing upwards. The external muscle layers were carefully peeled off the mucosa and pinned on Sylgard with longitudinal muscle side facing up.

Solutions and chemicals

The Ca^{2+} imaging bath chamber was constantly perfused with oxygenated KRB having the following composition (mM): NaCl 120.3, KCl 5.9, $MgCl_2$ 1.2, $NaHCO_3$ 15.5, NaH_2PO_4 1.2, glucose 11.5, $CaCl_2$ 2.5. The pH of the KRB was 7.3–7.4, when bubbled with 97% O_2/3% CO_2 at 37 $\pm$ 0.5°C. For the Ca^{2+} imaging experiments, nicardipine (Sigma, St Louis, MO, USA) was dissolved in ethanol at the stock concentration of 10 mM and added at a final concentration of 2–5 μM to block contractile activity. Niflumic acid (NFA) and 4,4′-diisothiocyanato-2,2′-stilbenedisulphonic acid disodium salt (DIDS) were purchased from Sigma; 5-nitro-2-(3-phenylpropylamino) benzoic acid (NPPB) was purchased from Tocris Biosciences (Ellisville, MO, USA). Stock of NFA (10 mM), DIDS (25 mM) and NPPB (25 mM) were prepared in dimethyl sulphoxide and all pharmacological stocks were added to the KRB at the desired concentrations and administered to the tissue via a constant perfusion system.

Calcium imaging

Fluo4 AM dye was used to visualize Ca^{2+} transients in ICC-MY. To determine if the cells showing oscillations in Fluo4 fluorescence were ICC-MY, we labelled live tissue with conjugated antibodies to Kit, a marker for ICC (Hanani *et al.* 1999). ACK2 (rat anti-mouse c-kit antibody; eBioscience, San Diego, CA, USA) was conjugated to Alexa Fluor 555 using an IgG labelling kit (Life Technologies, Carlsbad, CA, USA) as previously published for Alexa Fluor 488 conjugated ACK2 (Rich *et al.* 2002). Pinned tissue was incubated with conjugated ACK2 antibody for 1 h at 37°C in a CO_2 incubator. After washing twice with KRB, tissue was loaded with 5 μM Fluo4 AM and 0.02% Cremophor-EL (Sigma) for 30 min at room temperature in the dark. A wash out with KRB at 37°C was done in the perfusion chamber for 20 min to allow full de-esterification of AM esters.

Imaging and data analysis

Imaging was done on an upright Olympus confocal FV1000 microscope using a 20× water immersion objective (numerical aperture 0.95) with laser light excited at 488 nm to image Fluo4 and 543 nm for AF555-labelled ACK2. Single image frames were collected using the confocal aperture fully open. Data were analysed by measuring emitted fluorescence from regions of interest (ROI) over single ICC. The image files (16-bit, .tif) were analysed with ImageJ (version 1.46r) (Abramoff *et al.* 2004). Movements of the preparations were tracked using the Lucas–Kanade algorithm stabilizer routine and stabilized using a plugin for ImageJ. A walking average was applied to average the 8-bit intensity values of the adjacent frames to further reduce potential noise due to movement artefacts. Individual ROI representing Ca^{2+} induced fluorescence 'hot spots' were manually segmented using the ROI Manager tool in ImageJ. The average intensity value in each ROI was calculated for every frame. Care was taken to segment as closely to the boundary of each hot spot as possible, and to further reduce fluorescence contamination a background ROI that contained no calcium activity was subtracted from all the ROI containing Ca^{2+} activities.

Determination of transient coordination using synchonicity indices

The ROI intensity traces were exported and the peak values of each activity were detected using a Gaussian derivative-based peak detector in MATLAB (version R2011a). The time value corresponding to each peak value, i.e. the activation time, was collated and compared to the activation times in every other ROI in a round-robin manner in the same image stack using an event synchronization measurement (Quian Quiroga *et al.* 2002). A single synchronization index is reported between each pair of ROI (1 fully synchronous; 0 fully asynchronous). An event delay threshold of 600 ms was used to define whether two activation times were synchronous. The event delay threshold was based on four times the average time increment between frames (129 ms). In an image stack with M ROI, $M^*(M-1)/2$ synchronization values were reported and the average of these values was reported as the final synchronization index of the image stack. Based on the activation times,

the interval, frequency and amplitude values were also measured and reported as mean ± standard deviation.

Electrophysiology

Jejunum segments (about 10 mm long) from Ano1 WT and KO mice were removed and opened along the mesenteric border in KRB solution. Muscle strips with intact myenteric plexus were prepared by sharp dissection and pinned on Sylgard-coated custom made recording chambers (60 mm × 15 mm) with the circular muscle facing upward except for organotypic cultures where the recordings were made through longitudinal muscle. Muscles were pinned using fine wire pins (California Fine Wire Company, Grover Beach, CA, USA). Sharp microelectrode recordings were from circular smooth muscle cells. Glass capillary microelectrodes (borosilicate glass tube, 1.2 mm OD, 0.6 mm ID, 75 mm length, FHC Inc., Bowdoin, ME, USA) were pulled using a P-97 micropipette puller (Sutter Instruments, Novato, CA, USA). Microelectrodes filled with 3 M KCl had tip resistances ranging between 70 and 90 MΩ. Transmembrane potentials were measured using an Axoclamp 2B amplifier and a Digidata 1440A acquisition system, and stored on a computer running Axoscope 10.0 software (Axon Instruments/Molecular Devices Corp., Sunnyvale, CA, USA). Signals were recorded at a sampling rate of 2 kHz (interval of 500 μs). Muscle recording from Ano1 KO animals was confirmed by the presence of evoked inhibitory junction potentials. Electrical field stimulation was applied using two platinum wires placed perpendicular to the longitudinal axis of the preparation. The electrophysiological recording chamber was constantly perfused with oxygenated KRB solution aerated with 97% O_2/3% CO_2, and the pH of the solution was maintained at 7.3–7.4 at 37°C (±1°C). Muscles were allowed to equilibrate for 1–2 h before experiments were started. Electrical recordings were carried out in the presence of 2 μM nicardipine (Sigma) to minimize muscle contractility and to attain stable impalements.

Electrophysiological experiments were also done as described above on the muscle strips maintained in organotypic culture for lentiviral-mediated transduction with short hairpin RNA (shRNA)-NT and shRNA-Ano1. Electrical recordings were carried out in the presence of 4 μM nicardipine to minimize muscle contractility.

Data analysis for electrophysiology

Data were analysed off-line for (i) resting membrane potential, (ii) peak amplitude and (iii) frequency using Clampfit 10.3.1.5 software (Axon Instruments). In the organotypic culture tissues transduced with lenti-virus shRNA-NT and shRNA-Ano1 particles, recorded spontaneous electrical activity was accepted for analysis if a stable membrane potential was between −15 and −70 mV and the amplitude of the events was greater than 3 mV.

Organotypic culture and shRNA lentiviral transduction

The muscle layer of jejunum tissue from Ano1-WT mice was cultured as previously described (Ward *et al.* 1997; Mazzone *et al.* 2012). Briefly, tissues were loosely pinned (longitudinal muscle facing upwards) on a sterile Sylgard-coated dish. The muscles were washed with sterile culture medium at least five times and incubated at 37°C in a humidified atmosphere in M199 medium (Thermo Fisher, Waltham, MA, USA) supplemented with 5% fetal bovine serum (Thermo Fisher), glucose (4.5 g l^{-1}, Sigma), antibiotic–anti-mycotic mixture (pencillin G sodium, 200 i.u. ml^{-1}; streptomycin sulphate, 200 μg ml^{-1}; amphotericin B, 0.5 μg ml^{-1}; Thermo Fisher) plus L-glutamine (2 mM; Thermo Fisher). For shRNA lentiviral transduction, jejunum tissues (n = 6) were obtained from two mice from the same litter and organotypic cultures were maintained as described above. After 3 h of tissue equilibration in the CO_2 incubator, tissues were treated with non-targeting (NT) and shRNA Ano1 (n = 3) lentiviral transduction particles (mission-targeted shRNA lentiviral transduction particles for mouse Ano1 and NT lentiviral transduction particles from Sigma) with a multiplicity of infection (MOI) of 5. For the next 5 days, tissues were washed and fresh culture medium was added daily. After 5 days, one tissue each from shRNA NT and shRNA Ano1 was used for calcium imaging, one for electrical recording and one frozen immediately in liquid nitrogen for quantitative RT-PCR (qRT-PCR) to assess the knockdown of Ano1.

Immunohistochemistry

For Ano1 and Kit staining of muscle strips, organotypic cultures were washed with sterile PBS twice followed by fixation with cold acetone (4°C) for 15 min. Tissues were washed in PBS six times and incubated with 10% normal donkey serum (Jackson Immunoresearch Laboratories, West Grove, PA, USA) and 0.3% Triton-X-100 (Sigma) in PBS (4°C, overnight) to minimize non-specific antibody binding. Tissues were then incubated with ACK2 rat antibody (eBioscience, San Diego, CA, USA) and Ano1 rabbit antibody (Abcam, Cambridge, MA, USA) at 0.4 μg ml^{-1} in buffer (5% normal donkey serum, 2% BSA and 0.3% Triton-X-100) for 8 h at 4°C. Following washings in PBS, the tissues were incubated with donkey anti-rat Cy3 antibodies (Jackson Immunoresearch Laboratories) and donkey anti-rabbit FITC (Millipore, Billerica, MA,

USA). The labelled tissues were mounted using Slowfade mounting medium (Thermo Fisher). Whole-mounts were imaged using an upright Olympus confocal FV1000 microscope using a 20× water objective (numerical aperture 0.95) with laser light excited at 543 nm.

qRT-PCR

Total RNA was extracted from the frozen tissue using RNA-Bee isolation solvent (Tel-test Inc., Friendswood, TX, USA) following the manufacturer's instructions. Reverse transcription was done with a Superscript VILO cDNA synthesis kit (Life Technologies) using 200 ng of RNA and the reaction protocol consisted of annealing at 25°C for 10 min, followed by cDNA synthesis at 42°C for 60 min and the termination of reaction by incubation at 85°C for 5 min. The cDNA (14 ng) was then used for real-time PCR using LightCycler 480 SYBR Green I Master Mix (Roche, Indianapolis, IN, USA) with 250 nM of primers using the Roche LightCycler II. Primers for mouse Ano1 (PPM26917B) and β-actin (PPM02945A) were purchased from Qiagen (Valencia, CA, USA). All PCR reactions were done in a total volume of 25 μl with the following sequence: one cycle of initial denaturation for 5 min at 95°C and 45 amplification cycles (denaturation for 10 s at 95°C, annealing for 10 s at 60°C followed by extension for 10 s at 72°C). Expression of Ano1 was normalized to the endogenous control, β-actin, using the formula $\Delta\Delta C_t = [(Ct_{Ano1(shRNA\ Ano1)} - Ct_{\beta\text{-actin(shRNA Ano1)}})] - [(Ct_{Ano1(shRNA\ NT)} - Ct_{\beta\text{-actin(shRNA NT)}})]$ and the fold change is given by $2e^{-\Delta\Delta Ct}$, where C_t indicates the cycle number at which the fluorescence signal of the PCR product crosses an arbitrary threshold set within the exponential phase of the PCR amplification.

Contractility measurements

Horizontal organ bath chambers 10 ml in volume were used with normal KRB solution constantly aerated with a mixture of 97% oxygen and 3% carbon dioxide and maintained at 37 ± 0.5°C using an external water bath. Full thickness segments of jejunum 3 cm long were cut and tied at both ends with 5–0 surgical silk. The oral end of the segment was attached to a fixed point in the organ bath while the aboral end was attached to an isometric force displacement transducer (Grass Technologies, Warwick, RI, USA) used to measure contractile events. Initial tension load was set between 0.2 and 0.4 g, from which the segments would spontaneously relax over time, and the resting tone was adjusted when needed. Each segment was allowed to stabilize for 30 min before baseline contractions were recorded. The contractions were measured with isometric transducers connected to amplifiers (World Precision Instruments, Sarasota, FL, USA), and data were recorded with Acknowledge software (Biopac Systems, Goleta, CA, USA). The amplitude and frequency of the events were obtained from analysing 75 s of stable recordings from each tissue. The variation in amplitude and frequency between events was obtained from calculating the standard deviation/mean for these parameters between each event in the analysed trace. For all parameters means ± standard error of the mean (SEM) were calculated for five biological replicates. Data were analysed by exporting into Clampfit software.

Spatiotemporal mapping

Proximal small bowels of approximately 100 mm (duodenum and jejunum) were removed from littermates of Ano1 WT and Ano1 KO mice (PND 18–20). Luminal contents were flushed out. Segments were marked every 10–20 mm with India ink externally and were placed in an organ bath containing pre-warmed KRB at 37 ± 0.5°C. Intestines were cannulated at both ends to allow for measurement of intraluminal pressure and infusion of mucosal KRB with modifications as previously described (Bogeski *et al.* 2005). Briefly, the oral cannula was connected to a pressure transducer and a marriotte bottle filled with warm mucosal KRB solution. The aboral end was connected to a pressure transducer, a one-way valve (to prevent retrograde transport of fluid) and a fluid outlet to allow for the movement of fluid through the lumen. Segments were allowed to equilibrate for 30 min in an organ bath (75 ml volume) with perfusion rate of 10 ml min^{-1} to maintain the temperature of the organ bath. Baseline oral pressure was maintained at a constant value of 3 cmH_2O. Pressure readings were collected using pressure transducers connected to Transcribe4M and data were collected using Labscribe2 software. Spontaneous muscle contractility was recorded using avSony HDR-CX760 video camera mounted above the organ bath and spatiotemporal maps were constructed as described below.

Spatiotemporal map construction and analysis

QuickTime movies of intestinal preparations were decompressed and previewed in Volumetry G8a (author G.W.H.), calibrated for distance and time, then the region containing the intestine was cropped and imported as a stack at 8 frames s^{-1}. A maximum intensity projection was carried out to check if intestine remained within the cropped area during the entire movie. A threshold was applied to outline the intestine and small particles (usually air bubbles) were blacked out using a size particle filter ($<2 \times 2$ mm). The top and bottom edges of the preparation were identified, then a de-stub filter was applied

($dY/dX > 0.5$, 5 pixel span) to remove air bubble artefacts included in the upper and lower edge traces. The diameter between the top and bottom edges was calculated to create a spatiotemporal map (black indicated contraction, white dilation; see Fig. 9).

Statistics

Data are expressed as means ± SEM. Statistical significance was determined by Graphpad Prism using the appropriate statistical test. *P* values less than 0.05 were taken as a statistically significant difference. The '*n*' values refer to the number of animals.

Results

Effect of Ano1 on calcium transients using Ano1 knockout mice

Electrical recordings from jejunal circular smooth muscle cells from WT mice in the presence of the L-type calcium channel blocker nicardipine (2 μM) showed a typical electrical slow wave in smooth muscle cells whereas, as previously reported (Hwang *et al.* 2009), we were unable to record electrical slow waves in circular smooth muscle from Ano1 KO mouse jejunum ($n = 10$ mice, Fig. 1). In addition, the resting membrane potential for the recordings from the Ano1 KO mice was depolarized compared to the smooth muscle membrane potential in the Ano1 WT mice (Ano1 KO, −53.38 ± 4.26 mV; Ano1 WT, −62.83 ± 3.92 mV, mean ± SD, $n = 10$ mice, $P < 0.05$, unpaired *t* test).

The pacemaker signal in the small intestine arises from ICC-MY, which exhibit a robust Ca^{2+} transient (Hennig *et al.* 2002). We next recorded Ca^{2+} transients from ICC-MY from Ano1 WT and Ano1 KO mice. Ca^{2+} transients within the ICC network were visualized using the free intracellular Ca^{2+} binding dye Fluo4-AM, and to confirm that these events were occurring in ICC, we co-labelled the tissue with fluorescently labelled ACK-2 antibody to identify ICC (Fig. 2*A*). The analysed signals were from ROI that were confirmed to be coincident with Kit-positive, ICC-MY structures. These were the most prominent oscillating Fluo4 signals in each field. Some Kit-negative structures were also brightly loaded with Fluo4, including structures that resembled nerve fibres but these were excluded from this analysis of signals in the ICC-MY regions. The data do include signals from structures that were in the imaging plane but were above or below the Kit-labelled structure chosen for the ROI. The confocal aperture was fully open in these studies to avoid artefactual loss of signal caused by the ICC-MY in the ROI potentially moving out of the plane of focus despite the use of nicardipine. To control for signal from Kit-negative structures all images included analysis of a Kit negative region in each field. Spontaneous rhythmic Ca^{2+} transients were observed in ICC-MY from both Ano1 WT and Ano1 KO mice (Fig. 2*B* and *D*, supplementary movie S1). Due to the presence of nicardipine in the extracellular solutions we did not see significant propagation of the Ca^{2+} transients into the smooth muscle cells. However, whereas Ca^{2+} transients appeared coordinated within the ICC–MY network, on visual inspection of the real-time images from Ano1 WT mouse tissue, Ca^{2+} transients in Ano1 KO mouse tissue appeared uncoordinated. This is evident in the images of Fluo4 fluorescence; whereas all the ICC are bright in the single frame image from Ano1 WT tissue (Fig. 2*A*, left panel), only a proportion of the Kit-positive ICC fluoresce brightly at a single time point in the image from Ano1 KO tissue (Fig. 2*C*, left panel). We observed the same number of oscillating ICC-MY in the fields from Ano1 WT mice compared to Ano1 KO mice (11 ± 4 ICC per field in Ano1 KO *vs.* 13 ± 4 ICC per field in WT mice, $n = 8$ preparations each, $P =$ n.s., unpaired *t* test). The right panels in Fig. 2*A* and *C* show an overlay of the Kit signal and the Fluo4 signal for each image transformed to show the regions with the most oscillation in fluorescence signal to show how the oscillations were restricted to the regions of the Kit-positive ICC-MY. Using an event synchronization measurement, we analysed the coordination of the cytosolic Ca^{2+} transients (Fluo4 positive, left panel) from all ICC within microscopic fields (316.71 × 316.71 μm) in the ICC-MY region (Kit staining in right panel) from both Ano1 WT and KO mice (Fig. 2*B* and *D*, supplementary movie S2). Ca^{2+} transients in Ano1 WT mice were spontaneous, rhythmic and coordinated (Fig. 2*B* and supplementary movie S1) whereas Ca^{2+} transients within Ano1 KO mice were also spontaneous but not coordinated (Fig. 2*D* and supplementary movie S2). Ca^{2+} transients in ICC-MY from Ano1 KO mice were significantly less coordinated compared to Ano1 WT mice (0.362 ± 0.04 in Ano1 KO *vs.* 0.935 ± 0.03 in WT mice, $n = 8$ preparations each, $P < 0.05$, unpaired *t* test,

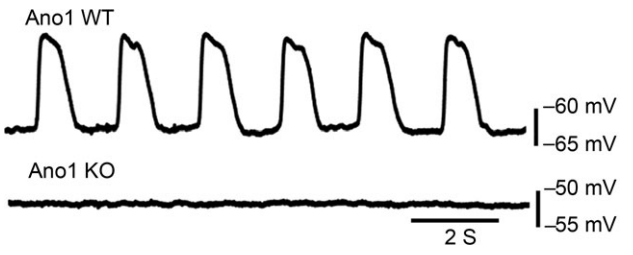

Figure 1. Slow waves were absent in Ano1 KO mice jejunum
Spontaneous electrical activity was recorded from jejunum muscularis propria of Ano1 WT and KO mice in the presence of 2 μM nicardipine using a sharp intracellular microelectrode. Representative traces from Ano1 WT (upper panel) and Ano1 KO (lower panel) are shown. Note the absence of slow waves (the rhythmic depolarization followed by a repolarization) in Ano1 KO mice.

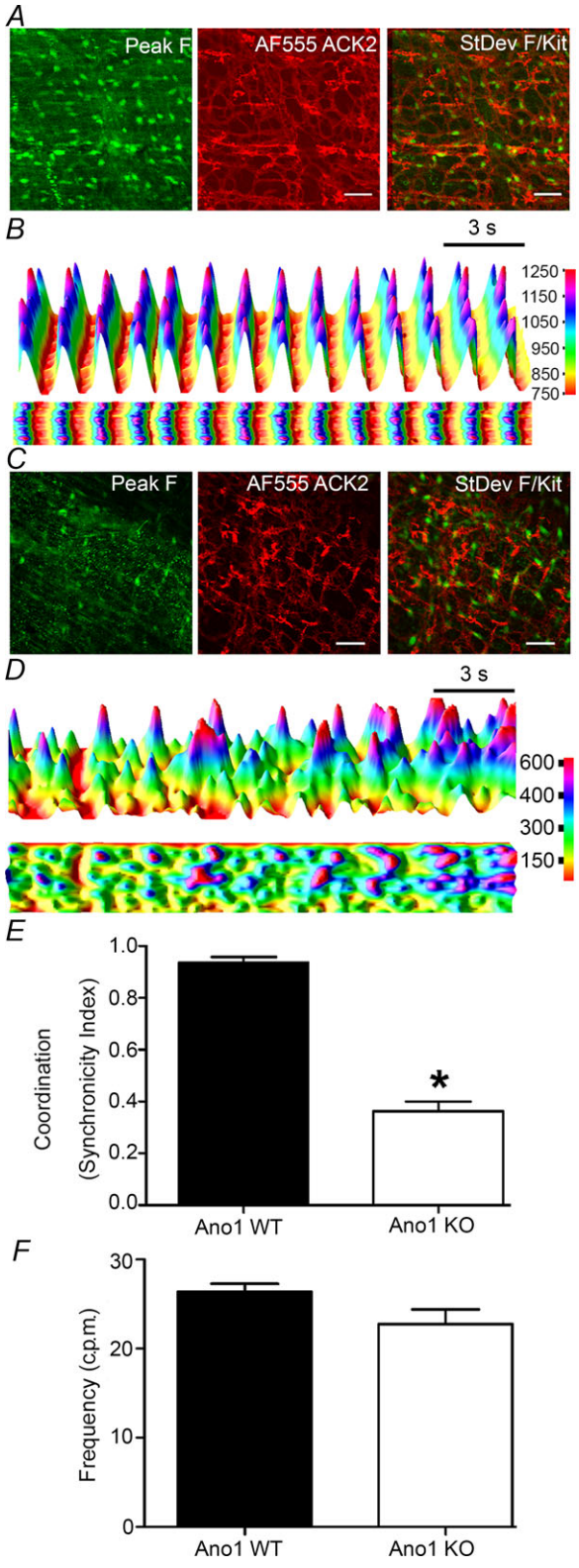

Figure 2. Loss of coordinated Ca^{2+} transients in ICC-MY of Ano1 KO mice
A, a representative image of Fluo4 labelling in ICC-MY (left) with the same area imaged to identify ICC-MY using AF555-labelled ACK2 (Kit) antibody (middle) in Ano1 WT mice. The right panel shows an image of the standard deviation in the fluorescence signal through the time series (green) overlaid with the Kit signal. Scale bar = 50 μm. *B*, fluorescence (arbitrary units) *vs.* time for Ca^{2+} transients from all the ICC present in the image showing rhythmic and coordinated Ca^{2+} transients in WT mice. The top panel shows the 3D projection of transients from top left to the right bottom of the Fluo4-labelled image (*A*) measured diagonally. The lower panel is a 2D image taken from the top of the 3D projection also indicating rhythmic and synchronous Ca^{2+} transients within the ICC network. *C*, representative image of Fluo4 labelling in ICC-MY (left) with the same area imaged to identify ICC-MY using AF555-labelled ACK2 (Kit) antibody (middle panel) in Ano1 KO mice. The right panel shows an image of the standard deviation in the fluorescence signal through the time series (green) overlaid with the Kit signal. Note that unlike *A*, not all the ICC-MY are brightly fluorescent at one time. Scale bar = 50 μm. *D*, the top panel shows the 3D projection of fluorescence (arbitrary units) *vs.* time for Ca^{2+} transients generated as for *B*. Note the uncoordinated Ca^{2+} transients within ICC-MY. The lower panel shows the 2D projection of Ca^{2+} transients again indicating the absence of coordination of Ca^{2+} transients from Ano1 KO mice. *E*, measurements in Ano1 WT and Ano1-KO tissues ($n = 8$; $^*P < 0.001$, *t* test) indicating loss of coordination of Ca^{2+} transients in ICC-MY of Ano1 KO mouse tissue as measured by the synchronicity index. *F*, frequency of ICC-MY Ca^{2+} transients from Ano1 WT and KO tissue was not significantly different ($n = 8$, P = n.s., *t* test).

Fig. 2*E*). There was no significant difference in Ca^{2+} transient frequency (26.38 ± 0.91 in WT *vs.* 22.75 ± 1.7 transients min^{-1} in Ano1 KO mice, $n = 8$ preparations each, P = n.s. unpaired *t* test, Fig. 2*F*).

Effect of chloride channel inhibitors on Ca^{2+} transients in Ano1 WT mice

To determine if the loss of Ca^{2+} transient coordination in Ano1 KO mice was due to loss of Cl^- transport *versus* an artefact associated with the constitutive knockout of Ano1 we next imaged Ca^{2+} transients in Ano1 WT mouse jejunum and acutely inhibited Ano1 activity using different pharmacological inhibitors. Given that currently available Cl^- channel blockers are relatively non-specific and no truly selective Ano1 channel blocker is available, we used three different inhibitors for this study: NFA (1 μM); NPPB (10 μM) and DIDS (10 μM). All three of these drugs have been reported to block slow wave activity in isolated and in intact ICC networks, although the effective concentration of the drugs varied even among different tissues in the same species (Hwang *et al.* 2009). In control experiments upon loading Fluo4 in Ano1 WT tissue, and imaging at time zero (0 min) and after 15 min, we did not observe a significant decrease in amplitude (78.5 ± 15.8 grey units at 0 min *vs.* 71.4 ± 18.5 at 15 min, $n = 3$ preparations, P = n.s., paired *t* test) and/or frequency of Ca^{2+} transients over time (24.8 ± 3.8 at 0 min *vs.* 24.2 ± 4.2 at 15 min, $n = 3$, P = n.s., paired *t* test, Fig. 3*A*). Treatment with pharmacological inhibitors of

Cl^- channels caused a loss of coordination in Ano1 WT tissue within 15 min of individual application of each of the three drugs (Fig. 3*B–D*). Treatment with NFA resulted in a significant decrease in transient coordination (0.90 ± 0.1 at 0 min *vs.* 0.18 ± 0.1 at 15 min, $n = 3$, $P < 0.05$, paired t test) and frequency (25.7 ± 3.8 at 0 min *vs.* 10.7 ± 3.06 at 15 min, $n = 3$, $P < 0.05$, paired t test) with no decrease in peak amplitude (50.7 ± 17.6 at 0 min *vs.* 28.4 ± 10.7 at 15 min, $n = 3$, $P =$ n.s., paired t test) (Fig. 3*E*). Treatment with DIDS resulted in a significant

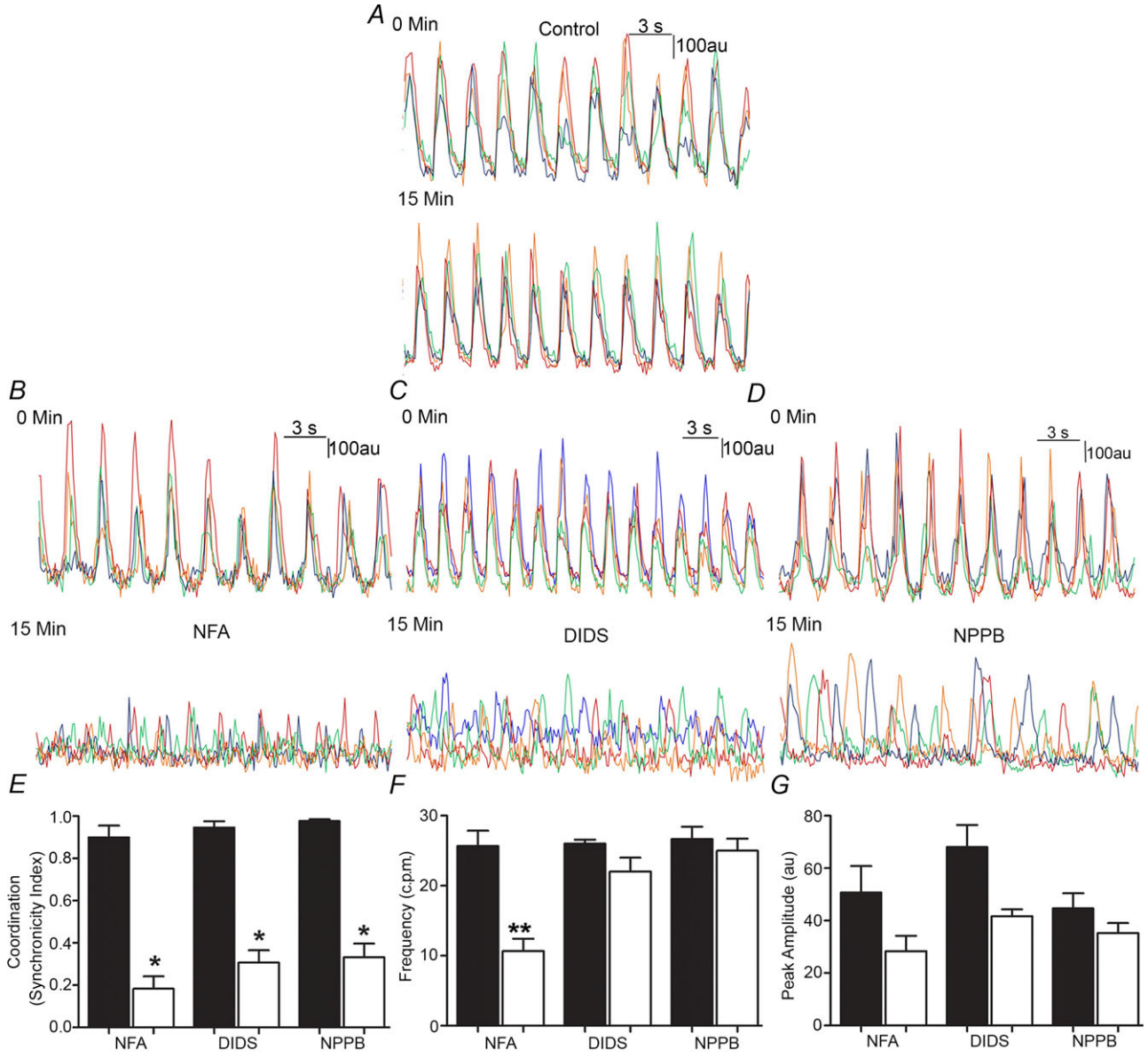

Figure 3. Loss of coordinated Ca^{2+} transients in Ano1 WT mice by pharmacological inhibitors of chloride channels

A, in control Ano1 WT tissue, representative traces from four different ICC showed no significant change in the amplitude or coordination of Ca^{2+} transients over 15 min. *B–D*, representative traces of Ca^{2+} transients upon pharmacological agent treatment showing the loss of coordinated Ca^{2+} transients in Ano1 WT tissue: 15 min treatment with NFA (1 μM, *B*), DIDS (10 μM, *C*) and NPPB (10 μM, *E*). *E*, measurements in Ano1 WT tissues upon treatment with NFA, DIDS and NPPB showed a significantly lower (*$P < 0.001$, paired t test) synchronicity index ($n = 3$). *F*, no significant difference in frequency was observed upon DIDS and NPPB treatment of Ano1 WT tissue, while significantly lower frequency (**$P < 0.05$, paired t test) was observed upon NFA treatment ($n = 3$). *G*, no significant difference in peak amplitude was observed upon pharmacological agent treatment of Ano1 WT tissue ($n = 3$, $P =$ n.s., paired t test).

decrease in transient coordination (0.93 ± 0.1 at 0 min *vs.* 0.31 ± 0.1 at 15 min, $n = 3$, $P < 0.05$, paired *t* test) with no decrease in frequency (26 ± 1.1 at 0 min *vs.* 22.1 ± 3.5 at 15 min, $n = 3$, $P =$ n.s., paired *t* test) and peak amplitude (68 ± 14.6 at 0 min *vs.* 41.7 ± 14.5 at 15 min, $n = 3$, $P =$ n.s., paired *t* test) (Fig. 3*F*). Treatment with NPPB also resulted in a significant decrease of coordination (0.97 ± 0.05 at 0 min *vs.* 0.33 ± 0.2 at 15 min, $n = 3$, $P < 0.05$, paired *t* test) with no decrease in frequency (26.7 ± 3.1 at 0 min *vs.* 25 ± 3.1 at 15 min, $n = 3$, $P =$ n.s., paired *t* test) and peak amplitude (44.7 ± 10.1 at 0 min *vs.* 35.33 ± 6.5 at 15 min, $n = 3$, $P =$ n.s., paired *t* test) (Fig. 3*G*).

These data suggest that we can replicate the constitutive Ano1 KO animal observations acutely using Cl^- channel inhibitors. Given the non-specific nature of these drugs as well as the possibility that they act on Cl^- conductances other than Ano1, we also tested these three drugs on Ca^{2+} transients in Ano1 KO mice. As reported above, Ca^{2+} transients in ICC-MY from Ano1 KO mice jejunum were not coordinated from the beginning and this lack of coordination was sustained up to 15 min. Synchronicity indices, frequency and peak amplitude were measured for each pharmacological agent as in Fig. 3 and no further significant changes were observed with any pharmacological agent over 15 min (Fig. 4*A*–*C*). Synchronicity indices for NFA treatment were 0.43 ± 0.1 at 0 min *vs.* 0.54 ± 0.2 at 15 min ($n = 3$, $P =$ n.s., paired *t* test), for DIDS treatment were 0.36 ± 0.12 at 0 min *vs.* 0.28 ± 0.09 at 15 min ($n = 3$, $P =$ n.s., paired *t* test) and for NPPB treatment were 0.32 ± 0.14 at 0 min *vs.* 0.30 ± 0.19 at 15 min ($n = 3$, $P =$ n.s., paired *t* test) (Fig. 4*D*). Frequency for NFA treatment was 22.0 ± 5.66 at 0 min *vs.* 21.1 ± 2.83 at 15 min ($n = 3$, $P =$ n.s., paired *t* test), for DIDS treatment was 21.1 ± 6.9 at 0 min *vs.* 19.4 ± 5.7 at 15 min ($n = 3$, $P =$ n.s., paired *t* test) and for NPPB treatment were 23 ± 2.1 at 0 min *vs.* 21.7 ± 2.1 at 15 min ($n = 3$, $P =$ n.s., paired *t* test) (Fig. 4*E*). Peak amplitude for NFA treatment was 55.5 ± 7.8 at 0 min *vs.* 29 ± 4.3 at 15 min ($n = 3$, $P =$ n.s., paired *t* test), for DIDS treatment was 66 ± 19.1 at 0 min *vs.* 50.4 ± 22.3 at 15 min ($n = 3$, $P =$ n.s., paired *t* test) and for NPPB treatment was 47.67 ± 15.5 at 0 min *vs.* 32 ± 8.7 at 15 min ($n = 3$, $P =$ n.s., paired *t* test) (Fig. 4*F*).

The lack of a further decrease in transient coordination after drug application in Ano1 KO mice is not conclusive evidence but suggests that the drug effect on coordination was indeed through Ano1. The Ca^{2+} transients in Ano1 KO tissue were absent after prolonged treatment (15–25 min) with these Cl^- channel inhibitor drugs, although this was also observed after prolonged treatment of WT tissues, suggesting that the inhibition of the individual Ca^{2+} transients seen in WT mice was probably not attributable to inhibition of Ano1.

Effect on Ca^{2+} transients of knocking down Ano1 expression using shRNA lentiviral particles

We next used an shRNA lentiviral approach to knock down Ano1 in organotypic culture. We first determined if we can maintain intact ICC networks, Ano1 expression and Ca^{2+} transient coordination in 5-day-old organotypic cultures. We prepared organotypic cultures from Ano1 WT mouse jejunum (12 days old), maintained these cultures for up to 5 days and used immunohistochemistry for Ano1 and Kit after 1 and 5 days in organotypic culture. We observed no significant changes in the ICC-MY network when labelled for Kit or Ano1 after 5 days in organotypic culture (Fig. 5). We next optimized the knockdown of Ano1 using Mission transduction shRNA-Ano1 and control shRNA-NT (non-targeting control shRNA) and determined that at an MOI of 5 after 5 days of treatment greater than 75% knockdown of Ano1 RNA expression was detected (using qRT-PCR, $n = 3$; $P < 0.05$ unpaired *t* test) (Fig. 6*A*). We then carried out Ca^{2+} imaging on the 5-day organotypic cultures. We observed normal coordinated Ca^{2+} transients in organotypic cultures with shRNA–NT whereas shRNA-Ano1 resulted in loss of coordination of the ICC Ca^{2+} transients (Fig. 6*B* and *C* and Supplementary movies S3 and S4). The same numbers of oscillating ICC per field were observed in the tissues treated with the non-targeting and Ano1-targeted shRNAs (10 ± 3 ICC per field for shRNA-NT *vs.* 10 ± 5 ICC per field in shRNA-Ano1 tissues, $n = 3$ preparations, $P =$ n.s., unpaired *t* test). These numbers were similar to the number of oscillating ICC detected in the freshly isolated tissues. Ca^{2+} transients in ICC-MY from Ano1 WT organotypic culture upon treatment with shRNA-Ano1 were significantly less coordinated compared to organotypic cultures treated with shRNA-NT (0.146 ± 0.04 in shRNA-Ano1 *vs.* 0.877 ± 0.05 in shRNA-NT, $n = 3$, $P < 0.05$, unpaired *t* test, Fig. 6*D*). There was no significant difference in Ca^{2+} transient frequency (13.57 ± 1.57 min^{-1} in Ano1 shRNA-Ano1 *vs.* 18.14 ± 1.61 min^{-1} in shRNA-NT, $n = 3$, $P =$ n.s., unpaired *t* test, Fig. 6*E*).

We also recorded electrical activity from organotypic cultures treated with shRNA-Ano1 and shRNA-NT (Fig. 7*A* and B). We observed a significant decrease in our ability to record slow wave activity in organotypic cultures treated with shRNA-Ano1. Slow waves were absent in ∼80% of the impaled smooth muscle cells (total impalements 211; $n = 3$) upon treatment with shRNA-Ano1, whereas slow waves were still present in ∼85% of the smooth muscle cell impalements (total impalements 239; $n = 3$; $P < 0.05$, χ^2 test) upon treatment with shRNA-NT (Fig. 7*C*). This transient knockdown of Ano1 had a similar effect on smooth muscle membrane potential as observed in Ano1 KO

mouse tissues in that tissues treated with shRNA-Ano1 were depolarized compared to the tissues treated with shRNA-NT (shRNA-Ano1, −34.62 ± 7.58 mV; shRNA-NT, −43.32 ± 5.68 mV, mean ± SD, $n = 3$ mice, $P < 0.05$, paired t test).

Effect of Ano1 on contractility of isolated small intestinal segments

Contractile activity in isolated small intestinal segments from Ano1 WT mice showed spontaneous rhythmic and coordinated contractility whereas under similar conditions significantly decreased contractility was observed in Ano1 KO mouse intestinal segments (Fig. 8*A* and *B*). Analysis of the tension recordings from Ano1 WT and Ano1 KO mice revealed a significantly higher amplitude of contractile force compared to Ano1 KO intestines (0.96 ± 0.21 mN in Ano1 WT *vs.* 0.16 ± 0.04 mN, $n = 5$, $P < 0.05$, unpaired t test, Fig. 8*C*). In addition, contractility appeared non-rhythmic and less coordinated in Ano1 KO intestinal segments. Overall, the frequency of the contractions was not different (0.60 ± 0.04 Hz in Ano1 WT *vs.* 0.55 ± 0.22 Hz in Ano1 KO, $n = 5$, n.s., unpaired t test, Fig. 8*E*) but there was a high degree of variation in the amplitude of the contractions in Ano1 KO intestines (0.13 ± 0.03 in Ano1 WT *vs.* 0.46 ± 0.09 in Ano1 KO, $n = 5$, $P < 0.05$, unpaired t test, Fig. 8*C* and *D*) and in variation of the frequency of the contractions (0.03 ± 0.02 in Ano1 WT *vs.* 0.52 ± 0.18 in Ano1 KO, $n = 5$, $P < 0.05$, unpaired t test, Fig. 8*F*). We therefore further analysed the patterns of motility from Ano1 WT and Ano1 KO proximal small intestinal (duodenum and jejunum) preparations from three mice each using spatiotemporal maps of contractility. Spatiotemporal maps showed regular ongoing, rhythmic contractions, previously referred to as 'ripples' in all the Ano1 WT intestinal preparations whereas these 'ripples' were irregular or short lived in all the Ano1 KO intestinal preparations (Fig. 9*A*). We also observed

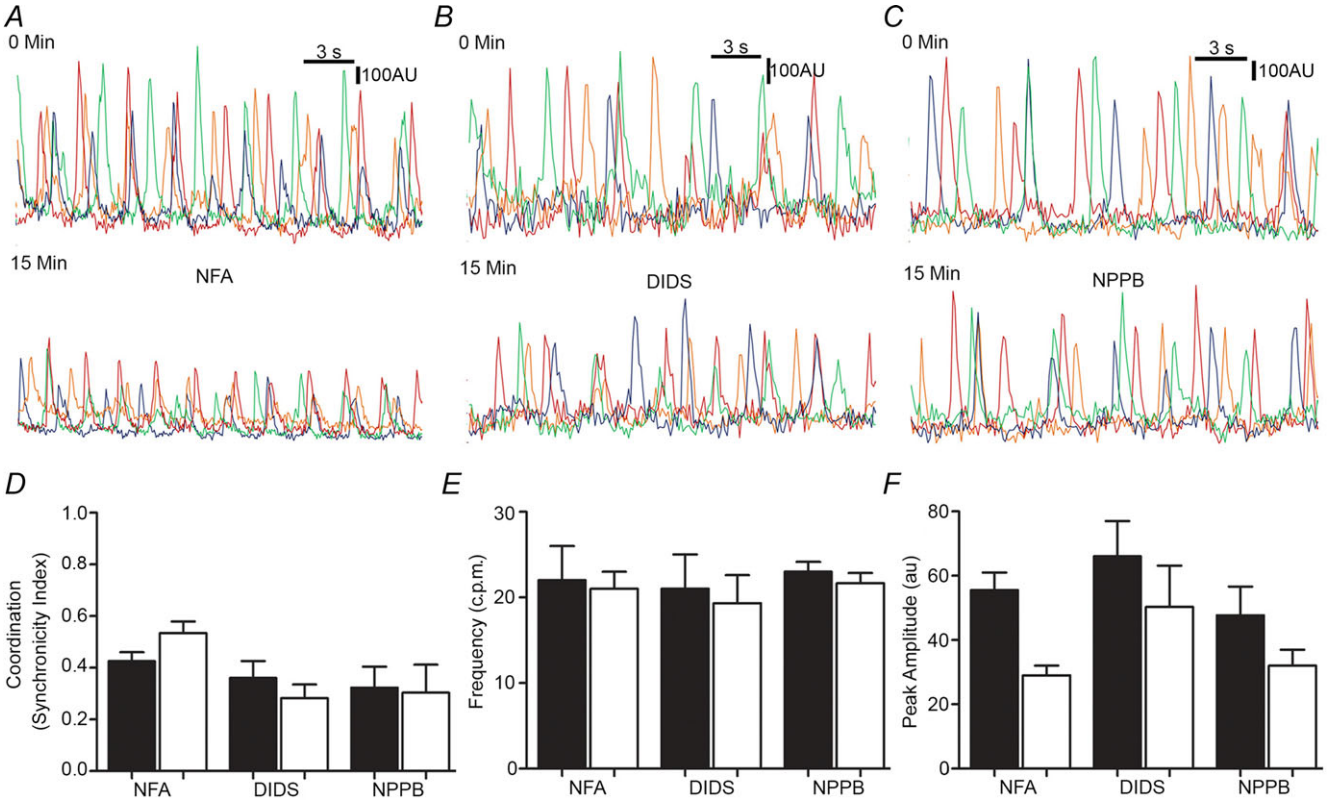

Figure 4. No further effects on Ca^{2+} transients with pharmacological inhibitors were observed in Ano1 KO mice
A–C, representative traces of Ca^{2+} transients upon pharmacological agent treatment in Ano1 KO tissue: 15 min treatment with NFA (1 μM, *A*), DIDS (10 μM, *B*) and NPPB (10 μM, *C*). *D*, measurements in Ano1 KO tissues upon treatment with NFA, DIDS and NPPB showed no significant difference in coordination of the events as indicated by the synchronicity index ($n = 3$, $P =$ n.s., paired t test). *E*, no significant difference in frequency was observed in Ano1 KO tissue upon treatment with NFA, DIDS and NPPB ($n = 3$, $P =$ n.s., paired t test). *F*, no significant difference in peak amplitude was observed in Ano1 KO tissue upon treatment with NFA, DIDS and NPPB ($n = 3$, $P =$ n.s., paired t test).

a superimposed phasic contractility happening every 90–120 s in Ano1 WT intestinal segments across the entire preparations, probably corresponding to synchronized contractile activity (black asterisks) (Fig. 9*B*). This contractile activity was still present in Ano1 KO preparations (black asterisks, Fig. 9*B*). Quantification of the frequency of the ongoing ripples in Ano1 WT and the brief periods of ripple-like activity in the Ano1 KO tissues indicated that the underlying frequencies were not different (Fig. 9*C*, 0.42 ± 0.18 Hz in Ano1 WT *vs.* 0.35 ± 0.04 Hz in Ano1 KO, $n = 3$, $P =$ n.s., unpaired *t* test).

Discussion

Coordinated phasic contractions of smooth muscle cells are required for gastrointestinal motor activities, including peristalsis and segmentation. Regulation of smooth muscle contractile activity occurs at many levels. The extrinsic nervous system modulates intrinsic nerve function. Enteric nerves generate stereotypic motor activity and also transduce environmental signals, including mechanical and chemical signals, into electrical signals that directly alter smooth muscle contractility (Kunze & Furness, 1999; Sanders, 2008). Enteric nerves also communicate to smooth muscle through ICC (Ward & Sanders, 2006). Other cell types also contribute to the regulation of smooth muscle contractility, including glia and enterochromaffin cells (Gershon & Tack, 2007; Savidge *et al.* 2007). The smooth muscle cell itself is also active in the regulation of contractile activity through mechanosensitive ion channels (Kraichely & Farrugia, 2007; Beyder & Farrugia, 2012) through signalling molecules (Horvath *et al.* 2006) and up and down regulation of various receptors in response to external input such as stretch and inflammation (Collins *et al.* 1994; Shi *et al.* 2011). These diverse cell types and signalling modalities need to be integrated to maintain coordination. ICC are one of the cell types that serve this role as they generate electrical slow waves (Szurszewski, 1987; Ward *et al.* 1994; Sanders, 1996) that are transmitted to smooth muscle cells and serve as a chronotropic contractile mechanism. Recent studies have shown that slow wave generation requires Ca^{2+}-activated Cl^- channels, probably by Ano1 in ICC of gastrointestinal muscles (Zhu *et al.* 2009). Mice lacking Ano1 do not have smooth muscle slow waves in the presence of L-type Ca^{2+} channel blockers, the electrical signal for which originates from ICC (Hwang *et al.* 2009). In the present study, we show that Ano1 has another major function in maintaining coordinated smooth muscle contractile activity by maintaining coordinated Ca^{2+} transients between ICC within the myenteric ICC network of the small intestine. Either genetic deletion of Ano1 in Ano1 KO mice, selective knock down in organotypic cultures or inhibition of Ano1 activity using pharmacological inhibitors resulted in loss of rhythmic and coordinated Ca^{2+} transients within the myenteric ICC network. As a result of loss of coordinated Ca^{2+} transients, the residual smooth muscle contractility is uncoordinated and irregular, as demonstrated by altered spatiotemporal maps in intact small intestinal preparations studied in the absence of L-type Ca^{2+} channel blockers.

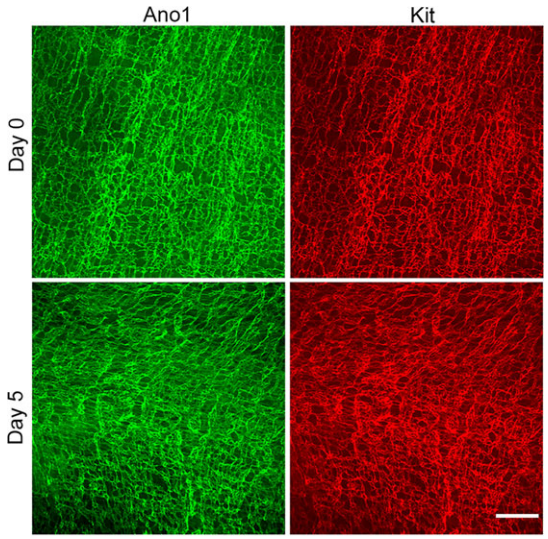

Figure 5. No change in Ano1 and Kit staining was observed in 5-day-old organotypic cultures
Organotypic cultures of smooth muscle layers from the jejunum of Ano1 WT mice were prepared and maintained for 5 days (see Methods). Tissues were immunolabelled for Ano1 and Kit at day 0 and day 5 after dissection. No difference in the density or distribution of Kit or Ano1 immunoreactivity was seen. Scale bar = 100 μm.

Our data suggest that Ano1 maintains the coordination of Ca^{2+} transients via the electrical signal generated by Cl^- movement through Ano1. Ano1, a Ca^{2+}-activated Cl^- channel, is expressed in ICC, and fluctuating levels of intracellular Ca^{2+} during Ca^{2+} transients in ICC-MY in turn regulate Ca^{2+}-sensitive ion channels that control membrane voltage, including Ano1. These interconnected signals can generate a self-regulating feedback loop that we propose maintains regularity of electrical and mechanical signalling. It will take innovative techniques to obtain voltage recordings directly from ICC, or better simultaneously from several ICC to prove this but several lines of evidence are presented here to support this concept. First, in constitutive Ano1 KO mice, while slow waves in smooth muscle were absent, Ca^{2+} transients were still present in ICC-MY occurring with a frequency similar to WT animals. However, Ca^{2+} transients in Ano1 KO mice were not coordinated between ICC in the myenteric plexus when compared to WT mice. Secondly, blocking Ano1 activity by using Cl^- channel inhibitors NFA, DIDS and NPPB also resulted in loss of temporal co-incidence of the ICC Ca^{2+} transients. These

inhibitors are non-specific and probably also act on other channels (discussed by Oh *et al.* 2008). We chose these three different Ca^{2+}-activated Cl^- channel inhibitors, NFA, DIDS and NPPB, because they have been shown to act as pharmacological inhibitors of Ca^{2+}-activated Cl^- channels and to block slow waves in smooth muscle (Koh *et al.* 2002; Hwang *et al.* 2009; Zhu *et al.* 2009). The mechanism by which they act as Ca^{2+}-activated Cl^- channel blockers is not well known but the off-target effects are varied (Oh *et al.* 2008). Concentration–response data from Ano1 channels expressed in HEK cells suggest more than 90% inhibition of currents by 10 μM NFA and DIDS (Yang *et al.* 2008). Selecting the right concentration of drug to use is important as concentrations at which the drugs act on different tissues, even within the same species, vary up to 30-fold; for example, the IC_{50} values for NFA and DIDS are 5.4 and 150 μM, respectively, for inhibition of slow waves in mouse colon while the IC_{50} values for NFA and DIDS are 150 and 1368 μM, respectively, for mouse small intestine (Hwang *et al.* 2009; Zhu *et al.* 2009). Effects of Ca^{2+}-activated Cl^- channel inhibitors have not been widely tested on the

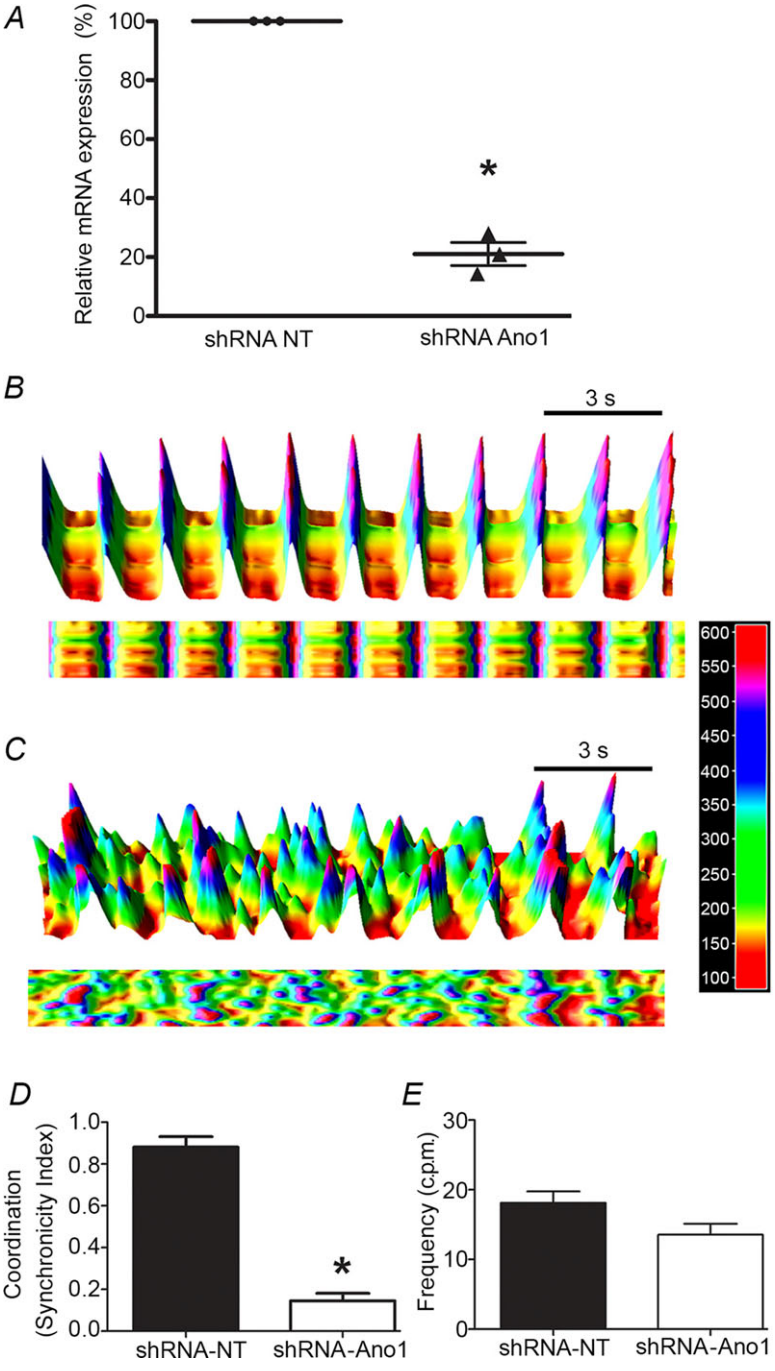

Figure 6. Ca^{2+} transients became uncoordinated upon transiently knocking down Ano1 in organotypic cultures
A, organotypic cultures were transduced with either non-targeting (NT) shRNA lentiviral particles or with shRNA lentiviral particles targeted to knock down Ano1 for 5 days. The relative mRNA expression of Ano1 upon transduction with non-targeting shRNA (represented as 100%) and upon transduction with shRNA-Ano1 upon normalization with β-actin (housekeeping gene). *B*, 3D projections of Ca^{2+} oscillations generated in organotypic cultures transduced with non-targeting shRNA lentiviral particles. Fluorescence (arbitrary units) *vs.* time is plotted. 2D projection of Ca^{2+} transients in lower panel shows rhythmic and coordinated Ca^{2+} transients within the ICC network. *C*, 3D projections of Ca^{2+} oscillations generated in organotypic cultures transduced with shRNA-Ano1. Fluorescence (arbitrary units) *vs.* time is plotted. 2D projection of Ca^{2+} transients in lower panel shows non-synchronous Ca^{2+} transients within the ICC network. *D*, measurements in Ano1 WT organotypic cultures upon shRNA-Ano1 transduction ($n = 3$) showed significantly less coordinated Ca^{2+} transients in ICC-MY (mean ± SEM, $n = 3$, $^*P < 0.001$, unpaired *t* test) when compared to organotypic cultures transduced with shRNA-NT as indicated by the synchronicity index. *E*, frequency of Ca^{2+} transients within Ano1 WT organotypic cultures upon shRNA-Ano1 and shRNA-NT transduction were not significantly different (mean ± SEM, $n = 3$, P = n.s., unpaired *t* test).

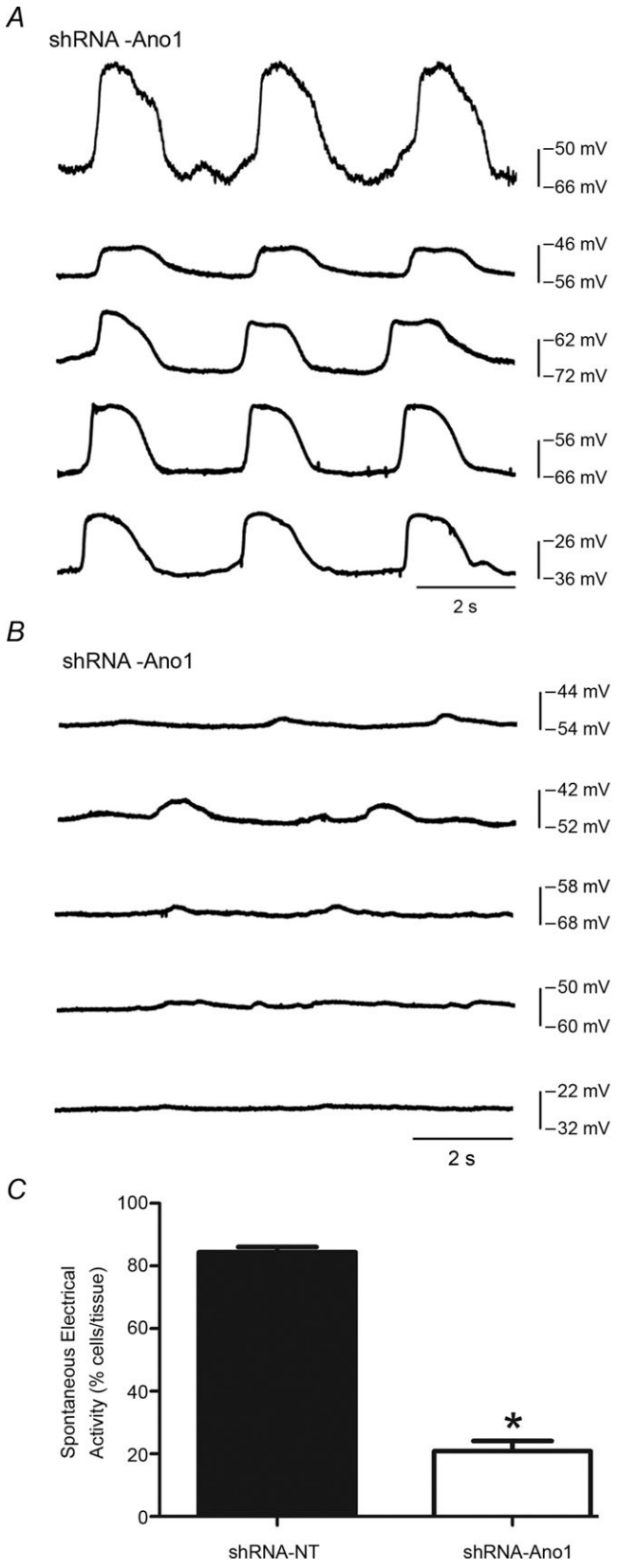

Figure 7. Reduced frequency of electrical slow waves in organotypic culture tissue upon transiently knocking down Ano1

A and *B*, intestinal tissues treated with shRNA-NT (*A*) and shRNA-Ano1 (*B*) for 5 days were analysed for electrical activity. Electrical recordings were made in the presence of 4 μM nicardipine. The figures show representative traces from five different cells from three different experiments. *C*, bar chart showing the average number of cells (as a percentage) exhibiting spontaneous electrical activity from shRNA-NT- and shRNA-Ano1-treated tissues. Spontaneous electrical activity (slow wave) was significantly reduced in shRNA-Ano1 KD tissue. Values are expressed as means ± SEM ($n = 3$, $^*P < 0.001$, unpaired *t* test).

Ca^{2+} transients in ICC-MY, although NFA (10 μM) has been shown to completely inhibit propagating Ca^{2+} waves within myosalpinx of mouse oviduct (Dixon *et al.* 2012). This complete inhibition obscured the possibility of detecting impairment of Ca^{2+} transient coordination. We chose substantially lower concentrations than the IC_{50} required to inhibit small intestinal slow waves. At these concentrations small intestinal ICC-MY Ca^{2+} transients became asynchronous. This effect did appear to be mediated predominantly through Ano1 as the blockers had no further effects on ICC-MY Ca^{2+} transients in Ano1 KO mice. In the present study, we also observed that longer exposure to these blockers resulted in complete loss of Ca^{2+} transients. However, this effect was also seen in Ano1 KO mice, suggesting it was a non-specific effect of the drugs. These data are notably consistent with NFA in particular having an effect on electrical slow waves that combine inhibition of Ano1 with block of other known targets, for example K^+ channels (Fernandez *et al.* 2008), and point to the need for care using the majority of currently available Cl^- channel blockers. The inhibition of Ca^{2+} transient amplitude with no further effect on coordination in Ano1 KO mice by all three drugs clearly indicates actions of the drug on targets that are not Ano1.

We also showed that ICC Ca^{2+} transients could be recorded from muscle strips and maintained for 20–25 min with no change in amplitude or frequency of the Ca^{2+} transients in the absence of drug treatment. This differs from previously reported results (Lowie *et al.* 2011) where a decrease in amplitude of ICC Ca^{2+} transients over the same time period was seen. This may be due to the fact that we used laser light of the confocal microscope at low intensity to excite Fluo4 (Lowie *et al.* 2011).

We knocked down Ano1 in organotypic cultures of isolated intact muscle layers isolated from Ano1 WT mice using lentiviral shRNA and observed that Ca^{2+} transients in organotypic cultures transduced with non-targeting shRNA lentiviral particles showed coordinated Ca^{2+} transients in ICC very similar to what we observed in freshly isolated tissues from Ano1 WT mice. In contrast, ICC Ca^{2+} transients from organotypic cultures transduced with shRNA lentiviral particles for Ano1 exhibited Ca^{2+} transients that were not coordinated as we observed in Ano1 KO mice. Therefore, acute selective knockdown of

Ano1 had the same effect as chronic loss of or non-selective block of Ano1. These data taken together strongly suggest that Ano1 is required for coordination of Ca^{2+} transients between ICC in the myenteric region of the small intestine of mice.

The transient knockdown of Ano1 using shRNA also reproduced a depolarization of membrane voltage that we observed in tissues from Ano1 KO tissues and which is apparent but not discussed in the study by Hwang *et al.* (2009) on Ano1 KO mice. This depolarization is consistent with a role for functional ICC-MY contributing to the membrane potential in circular smooth muscle of the small intestine (Ward *et al.* 1994; Farrugia *et al.* 2003). As discussed above, innovative methods for recording

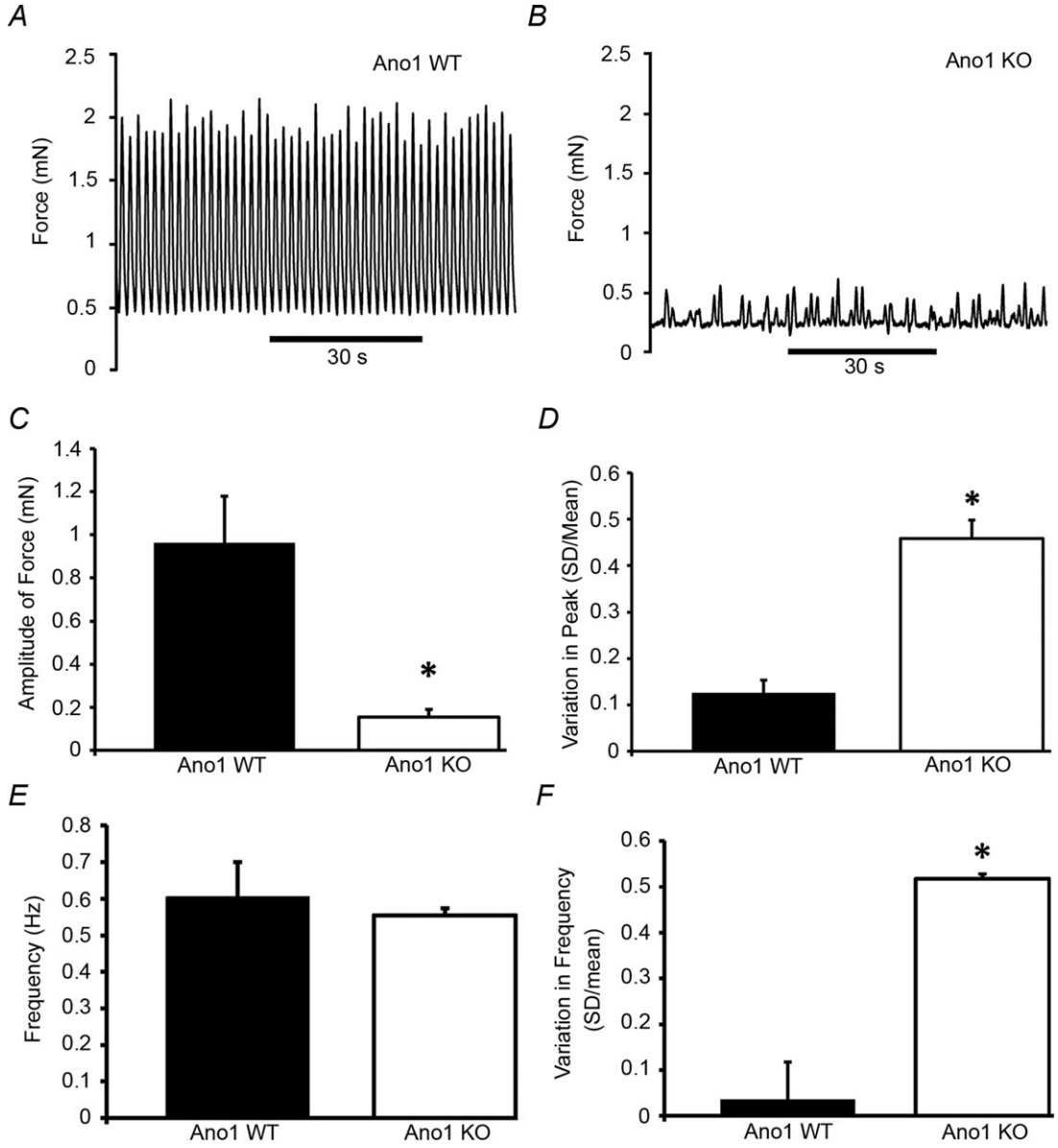

Figure 8. Absence of Ano1 causes an uncoordinated contractile pattern in Ano1 KO mouse small intestine

A, representative tension recordings of isolated small intestines from Ano1 WT and Ano1 KO tissue. Patterns of intestinal contractility from Ano1 WT (*A*) and Ano1 KO mice (*B*) are shown. Note the significantly lower tension force in the Ano1 KO tissue. *C*, quantification of the amplitude of force tension recordings revealed a significantly lower amplitude of force in Ano1 KO mice ($n = 5$, $^*P < 0.05$, unpaired *t* test). *D*, variation in the peak amplitude of force between individual events was determined using SD/mean of events and revealed a significantly higher variation in peak amplitude of force ($n = 5$; $^*P < 0.05$, unpaired *t* test). *E*, no significant differences in the overall frequency of events in Ano1 WT and Ano1 KO mice were observed ($n = 5$). *F*, variation in the instantaneous frequency of events within each trace as determined by SD/mean was significantly higher in Ano1 KO mice ($n = 5$, $^*P < 0.05$, unpaired *t* test).

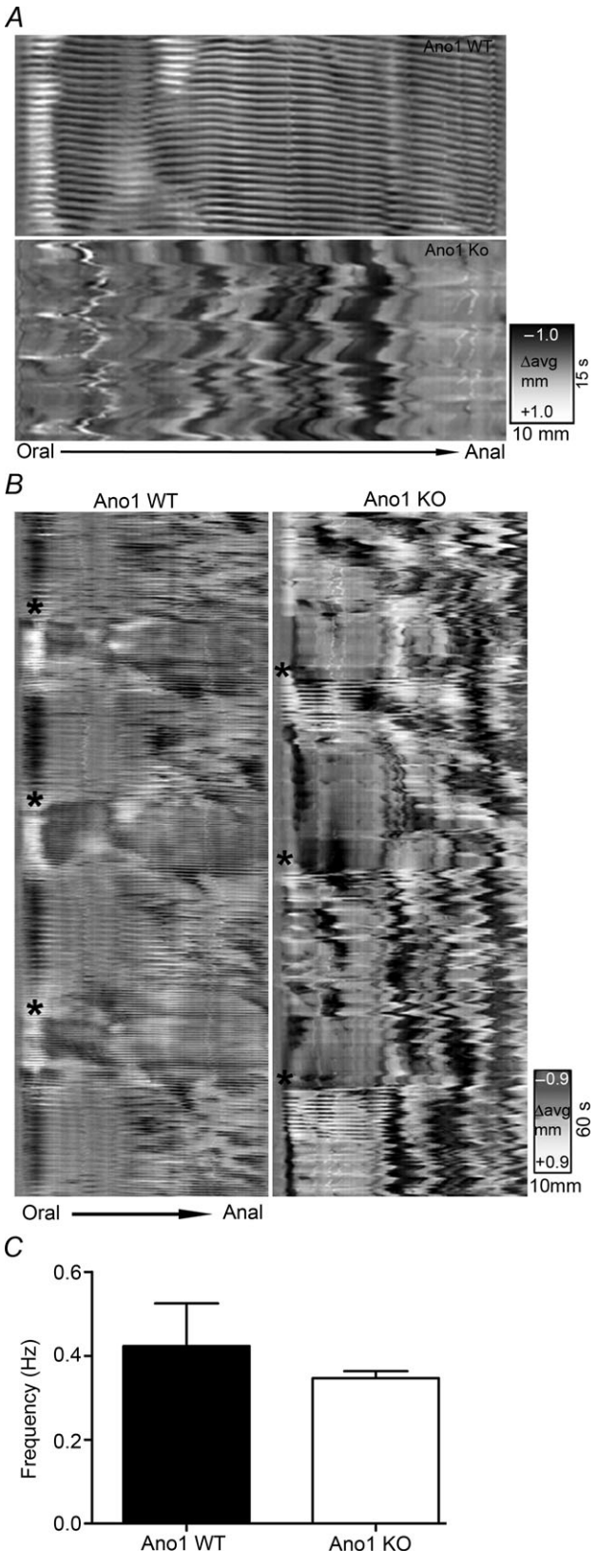

membrane voltage in both ICC and smooth muscle are necessary to establish if and how changes to ICC membrane voltage couple to changes in smooth muscle cell membrane voltage in response to Ano1 knockout. It is unlikely that this depolarization alone is sufficient to cause loss of the slow wave as KO mice lacking both heme oxygenase 2 and neuronal nitric oxide synthase have more depolarized smooth muscle membrane potentials than reported here and retain slow wave activity (Xue *et al.* 2000).

For electrical slow wave activity to couple to effective and coordinated contractile activity in the muscle layers of the mouse small intestine, the electrical signal needs to be synchronous and to propagate in an organized fashion through the tissue. In rodents, propagation of this activity has been demonstrated in studies on rodent small intestine to occur with a speed of about 4 mm s^{-1} for electrical activity recorded extracellularly in rat jejunum (Lammers *et al.* 2011) and 10 mm s^{-1} for the wave front of Ca transients in ICC-MY from mouse ileum (Park *et al.* 2006). This gives a window of between 30 and 75 ms for the activity to propagate across our images, which have a dimension of 0.3 × 0.3 mm. We collected data with a sampling rate of 130 ms so it was technically impossible for us to collect data fast enough to detect propagation of the Ca^{2+} transients or to establish any directional component to the propagation. However, the resolution was sufficient to ensure that the Ca^{2+} transients with a frequency of one per 2.6 s were not aliased and that the observed absence of coordinated Ca^{2+} transient in tissues with no or inhibited Ano1 activity reflected a genuine loss of a mechanism for synchronizing the events. We propose that Cl^- movement through Ano1 channels in ICC is a mechanism for entraining or synchronizing the Ca^{2+} transients and associated pacemaker potentials. The profound change that we observed in the coordination of the Ca^{2+} transients following removal or inhibition of Ano1 activity is consistent with Ano1 playing this

Figure 9. Altered spatiotemporal maps in Ano1 KO mice small intestines
Representative images of patterns of motility from Ano1 WT and Ano1 KO mouse small intestinal preparation. *A*, the spatiotemporal maps (top) from an Ano1 WT mouse exhibiting regular and rhythmic contractions (referred to as 'ripples') whereas in Ano1 KO (bottom) showed absence of ripple activity signifying loss of rhythmic synchronized contractile activity. *B*, representative spatiotemporal maps on a lower scale from Ano1 WT mice (left) again showing ripples and also showing a phasic modulation of contractility across the entire preparation, probably corresponding to synchronized contractile activity (black asterisks). The right panel again shows uncoordinated ripples and shows that phasic modulation of contractile activity still appeared to be present (black asterisks) in Ano1 KO preparations. *C*, spatiotemporal map analysis revealed no significant difference in frequency of contractions in Ano1 WT and Ano1 KO mice (mean ± SEM, $n = 3$, P = n.s., unpaired t test).

proposed role. The net result of loss of coordinated ICC-MY Ca^{2+} transients was loss of coordination of smooth muscle contractile behaviour. We measured contractility in isolated intact small intestines and constructed spatiotemporal maps to examine contractile patterns. Preparations from small intestines from Ano1 KO mice showed significantly decreased contractility mostly due to decreased contraction amplitude at similar frequencies, probably a result of the smaller depolarizing slow wave resulting in less Ca^{2+} entry through L-type Ca^{2+} channels (Farrugia, 1999). Contractility was also non-rhythmic and less coordinated in Ano1 KO small intestine segments. Spatiotemporal maps from Ano1 WT showed a prominent and consistent ripple pattern that reflects propagating contractions as first described in the mouse colon (Roberts *et al.* 2007). These ripples were either not clearly seen or absent in Ano1 KO small intestines, suggesting that smooth muscle contractile activity was indeed uncoordinated and unable to produce a measurable coordinated contractile front. In contrast to the loss of the 'ripples' there were regular periods of coordinated contractile activity that were picked up by the spatiotemporal maps. These probably reflect intrinsic nerve communication to smooth muscle generating the synchronized contractile activity.

In summary, we propose a novel role for the Ca^{2+}-activated Cl^- channel Ano1 in maintaining coordinated Ca^{2+} transients in ICC-MY. Despite the ICC networks being intact, loss of Ano1 resulted in uncoordinated Ca^{2+} transients between ICC in the myenteric region and in uncoordinated contractile activity in intact small intestine segments. This finding expands our understanding of the role of Ano1 and opens the possibility that a similar function may be operative in other contractile tissues where Ano1 is expressed.

References

Abramoff MD, Magalhaes PJ & Ram SJ (2004). Image processing with ImageJ. *Biophotonics Int* **11**, 7.

Berg J, Yang H & Jan LY (2012). Ca^{2+}-activated Cl^- channels at a glance. *J Cell Sci* **125**, 1367–1371.

Beyder A & Farrugia G (2012). Targeting ion channels for the treatment of gastrointestinal motility disorders. *Therap Adv Gastroenterol* **5**, 5–21.

Bogeski G, Shafton AD, Kitchener PD, Ferens DM & Furness JB (2005). A quantitative approach to recording peristaltic activity from segments of rat small intestine in vivo. *Neurogastroenterol Motil* **17**, 262–272.

Bulley S & Jaggar JH (2013). Cl channels in smooth muscle cells. *Pflugers Arch* **466**, 861–872.

Collins SM, Khan I, Vallance B & Hogaboam C (1994). The role of smooth muscle in intestinal inflammation. In *Inflammatory Bowel Disease Basic Research, Clinical Implications and Trends in Therapy*, ed. Sutherland LR, Collins SM, Martin F, McLeod RS & Targan SR, pp. 162–169. Springer, Dordrecht.

Dixon RE, Hennig GW, Baker SA, Britton FC, Harfe BD, Rock JR, Sanders KM & Ward SM (2012). Electrical slow waves in the mouse oviduct are dependent upon a calcium activated chloride conductance encoded by *Tmem16a*. *Biol Reprod* **86**, 1–7.

Farrugia G (1999). Ionic conductances in gastrointestinal smooth muscles and interstitial cells of Cajal. *Annu Rev Physiol* **61**, 45–84.

Farrugia G, Lei S, Lin X, Miller SM, Nath KA, Ferris CD, Levitt M & Szurszewski JH (2003). A major role for carbon monoxide as an endogenous hyperpolarizing factor in the gastrointestinal tract. *Proc Natl Acad Sci U S A* **100**, 8567–8570.

Fernandez D, Sargent J, Sachse FB & Sanguinetti MC (2008). Structural basis for ether-a-go-go-related gene K^+ channel subtype-dependent activation by niflumic acid. *Mol Pharmacol* **73**, 1159–1167.

Gershon MD & Tack J (2007). The serotonin signaling system: from basic understanding to drug development for functional GI disorders. *Gastroenterology* **132**, 397–414.

Gomez-Pinilla PJ, Gibbons SJ, Bardsley MR, Lorincz A, Pozo MJ, Pasricha PJ, de Rijn MV, West RB, Sarr MG, Kendrick ML, Cima RR, Dozois EJ, Larson DW, Ordog T & Farrugia G (2009). Ano1 is a selective marker of interstitial cells of Cajal in the human and mouse gastrointestinal tract. *Am J Physiol Gastrointest Liver Physiol* **296**, G1370–G1381.

Hanani M, Belzer V, Rich A & Faussone-Pellegrini SM (1999). Visualization of interstitial cells of Cajal in living, intact tissues. *Microsc Res Tech* **47**, 336–343.

Hennig GW, Smith CB, O'Shea DM & Smith TK (2002). Patterns of intracellular and intercellular Ca^{2+} waves in the longitudinal muscle layer of the murine large intestine *in vitro*. *J Physiol* **543**, 233–253.

Horvath VJ, Vittal H, Lorincz A, Chen H, Almeida-Porada G, Redelman D & Ordog T (2006). Reduced stem cell factor links smooth myopathy and loss of interstitial cells of Cajal in murine diabetic gastroparesis. *Gastroenterology* **130**, 759–770.

Huizinga JD, Thuneberg L, Kluppel M, Malysz J, Mikkelsen HB & Bernstein A (1995). *W/kit* gene required for interstitial cells of Cajal and for intestinal pacemaker activity. *Nature* **373**, 347–349.

Hwang SJ, Blair PJ, Britton FC, O'Driscoll KE, Hennig G, Bayguinov YR, Rock JR, Harfe BD, Sanders KM & Ward SM (2009). Expression of anoctamin 1/TMEM16A by interstitial cells of Cajal is fundamental for slow wave activity in gastrointestinal muscles. *J Physiol* **587**, 4887–4904.

Koh SD, Jun JY, Kim TW & Sanders KM (2002). A Ca^{2+}-inhibited non-selective cation conductance contributes to pacemaker currents in mouse interstitial cell of Cajal. *J Physiol* **540**, 803–814.

Kraichely RE & Farrugia G (2007). Mechanosensitive ion channels in interstitial cells of Cajal and smooth muscle of the gastrointestinal tract. *Neurogastroenterol Motil* **19**, 245–252.

Kunze WA & Furness JB (1999). The enteric nervous system and regulation of intestinal motility. *Annu Rev Physiol* **61**, 117–142.

Kunzelmann K, Tian Y, Martins JR, Faria D, Kongsuphol P, Ousingsawat J, Wolf L & Schreiber R (2012). Airway epithelial cells–functional links between CFTR and anoctamin dependent Cl^- secretion. *Int J Biochem Cell Biol* **44**, 1897–1900.

Lammers WJ, Al-Bloushi HM, Al-Eisaei SA, Al-Dhaheri FA, Stephen B, John R, Dhanasekaran S & Karam SM (2011). Slow wave propagation and plasticity of interstitial cells of Cajal in the small intestine of diabetic rats. *Exp Physiol* **96**, 1039–1048.

Lowie BJ, Wang XY, White EJ & Huizinga JD (2011). On the origin of rhythmic calcium transients in the ICC-MP of the mouse small intestine. *Am J Physiol Gastrointest Liver Physiol* **301**, 11.

Martins JR, Faria D, Kongsuphol P, Reisch B, Schreiber R & Kunzelmann K (2011). Anoctamin 6 is an essential component of the outwardly rectifying chloride channel. *Proc Natl Acad Sci U S A* **108**, 18168–18172.

Mazzone A, Eisenman ST, Strege PR, Yao Z, Ordog T, Gibbons SJ & Farrugia G (2012). Inhibition of cell proliferation by a selective inhibitor of the Ca(2+)-activated Cl(−) channel, Ano1. *Biochem Biophys Res Commun* **427**, 248–253.

Oh SJ, Park JH, Han S, Lee JK, Roh EJ & Lee CJ (2008). Development of selective blockers for Ca^{2+}-activated Cl channel using *Xenopus laevis* oocytes with an improved drug screening strategy. *Mol Brain* **1**, 1756–6606.

Park KJ, Hennig GW, Lee HT, Spencer NJ, Ward SM, Smith TK & Sanders KM (2006). Spatial and temporal mapping of pacemaker activity in interstitial cells of Cajal in mouse ileum *in situ*. *Am J Physiol Cell Physiol* **290**, 28.

Quian Quiroga R, Kreuz T & Grassberger P (2002). Event synchronization: a simple and fast method to measure synchronicity and time delay patterns. *Phys Rev E Stat Nonlin Soft Matter Phys* **66**, 15.

Rich A, Hanani M, Ermilov LG, Malysz J, Belzer V, Szurszewski JH & Farrugia G (2002). Physiological study of interstitial cells of Cajal identified by vital staining. *Neurogastroenterol Motil* **14**, 189–196.

Roberts RR, Murphy JF, Young HM & Bornstein JC (2007). Development of colonic motility in the neonatal mouse-studies using spatiotemporal maps. *Am J Physiol Gastrointest Liver Physiol* **292**, G930–G938.

Rock JR, Futtner CR & Harfe BD (2008). The transmembrane protein TMEM16A is required for normal development of the murine trachea. *Dev Biol* **321**, 141–149.

Sagheddu C, Boccaccio A, Dibattista M, Montani G, Tirindelli R & Menini A (2010). Calcium concentration jumps reveal dynamic ion selectivity of calcium-activated chloride currents in mouse olfactory sensory neurons and TMEM16b-transfected HEK 293T cells. *J Physiol* **588**, 4189–4204.

Sanders KM (1996). A case for interstitial cells of Cajal as pacemakers and mediators of neurotransmission in the gastrointestinal tract. *Gastroenterology* **111**, 492–515.

Sanders KM (2008). Regulation of smooth muscle excitation and contraction. *Neurogastroenterol Motil* **20**, 39–53.

Savidge TC, Newman P, Pothoulakis C, Ruhl A, Neunlist M, Bourreille A, Hurst R & Sofroniew MV (2007). Enteric glia regulate intestinal barrier function and inflammation via release of *S*-nitrosoglutathione. *Gastroenterology* **132**, 1344–1358.

Schreiber R, Uliyakina I, Kongsuphol P, Warth R, Mirza M, Martins JR & Kunzelmann K (2010). Expression and function of epithelial anoctamins. *J Biol Chem* **285**, 7838–7845.

Schroeder BC, Cheng T, Jan YN & Jan LY (2008). Expression cloning of TMEM16A as a calcium-activated chloride channel subunit. *Cell* **134**, 1019–1029.

Shi XZ, Lin YM, Powell DW & Sarna SK (2011). Pathophysiology of motility dysfunction in bowel obstruction: role of stretch-induced COX-2. *Am J Physiol Gastrointest Liver Physiol* **300**, G99–G108.

Stanich JE, Gibbons SJ, Eisenman ST, Bardsley MR, Rock JR, Harfe BD, Ordog T & Farrugia G (2011). Ano1 as a regulator of proliferation. *Am J Physiol Gastrointest Liver Physiol* **301**, G1044–G1051.

Stephan AB, Shum EY, Hirsh S, Cygnar KD, Reisert J & Zhao H (2009). ANO2 is the cilial calcium-activated chloride channel that may mediate olfactory amplification. *Proc Natl Acad Sci U S A* **106**, 11776–11781.

Szurszewski JH (1987). Electrophysiological basis of gastrointestinal motility. In *Physiology of the Gastrointestinal Tract*, 2nd edn, ed. Johnson LR, pp. 383–422. Raven Press, New York.

Thuneberg L (1982). Interstitial cells of Cajal: intestinal pacemaker cells? *Adv Anat Embryol Cell Biol* **71**, 1–130.

Tian Y, Schreiber R & Kunzelmann K (2012). Anoctamins are a family of Ca^{2+}-activated Cl^- channels. *J Cell Sci* **125**, 4991–4998.

Torihashi S, Fujimoto T, Trost C & Nakayama S (2002). Calcium oscillation linked to pacemaking of interstitial cells of Cajal: requirement of calcium influx and localization of TRP4 in caveolae. *J Biol Chem* **277**, 19191–19197.

Torihashi S, Ward SM, Nishikawa S, Nishi K, Kobayashi S & Sanders KM (1995). c-kit-dependent development of interstitial cells and electrical activity in the murine gastrointestinal tract. *Cell Tissue Res* **280**, 97–111.

Tran TT, Tobiume K, Hirono C, Fujimoto S, Mizuta K, Kubozono K, Inoue H, Itakura M, Sugita M & Kamata N (2014). TMEM16E (GDD1) exhibits protein instability and distinct characteristics in chloride channel/pore forming ability. *J Cell Physiol* **229**, 181–190.

Ward SM, Beckett EA, Wang X, Baker F, Khoyi M & Sanders KM (2000). Interstitial cells of Cajal mediate cholinergic neurotransmission from enteric motor neurons. *J Neurosci* **20**, 1393–1403.

Ward SM, Burns AJ, Torihashi S & Sanders KM (1994). Mutation of the proto-oncogene c-*kit* blocks development of interstitial cells and electrical rhythmicity in murine intestine. *J Physiol* **480**, 91–97.

Ward SM, Harney SC, Bayguinov JR, McLaren GJ & Sanders KM (1997). Development of electrical rhythmicity in the murine gastrointestinal tract is specifically encoded in the tunica muscularis. *J Physiol* **505**, 241–258.

Ward SM & Sanders KM (2006). Involvement of intramuscular interstitial cells of Cajal in neuroeffector transmission in the gastrointestinal tract. *J Physiol* **576**, 675–682.

Xue L, Farrugia G, Miller SM, Ferris CD, Snyder SH & Szurszewski JH (2000). Carbon monoxide and nitric oxide as coneurotransmitters in the enteric nervous system: evidence from genomic deletion of biosynthetic enzymes. *Proc Natl Acad Sci U S A* **97**, 1851–1855.

Yamazawa T & Iino M (2002). Simultaneous imaging of Ca^{2+} signals in interstitial cells of Cajal and longitudinal smooth muscle cells during rhythmic activity in mouse ileum. *J Physiol* **538**, 823–835.

Yang H, Kim A, David T, Palmer D, Jin T, Tien J, Huang F, Cheng T, Coughlin SR, Jan YN & Jan LY (2012). TMEM16F forms a Ca^{2+}-activated cation channel required for lipid scrambling in platelets during blood coagulation. *Cell* **151**, 111–122.

Yang YD, Cho H, Koo JY, Tak MH, Cho Y, Shim WS, Park SP, Lee J, Lee B, Kim BM, Raouf R, Shin YK & Oh U (2008). TMEM16A confers receptor-activated calcium-dependent chloride conductance. *Nature* **455**, 1210–1215.

Zhu MH, Kim TW, Ro S, Yan W, Ward SM, Koh SD & Sanders KM (2009). A Ca^{2+}-activated Cl^- conductance in interstitial cells of Cajal linked to slow wave currents and pacemaker activity. *J Physiol* **587**, 4905–4918.

Additional Information

Competing interests

The authors declare that they have no competing interests or conflicts of interest with respect to this work.

Author contributions

This work was done in the laboratory of G.F. R.D.S., S.J.G. and G.F. were involved in the conception and design of the experiments. R.D.S., S.J.G., S.A.S., P.D., G.W.H., S.T.E., A.M., Y.H., C.C., G.J.S., J.R.R., B.D.H. and G.F. were involved in collection analysis and interpretation of the data. R.D.S., S.J.G., S.A.S., P.D., G.W.H., Y.H., T.O., J.H.S. and G.F. were involved in drafting the article or revising it critically for important intellectual content. All authors approved the final version of the manuscript. All persons designated as authors qualify for authorship and all those who qualify for authorship are listed.

Funding

This work was supported by NIH grant DK57061. P.D. is supported by a New Zealand Postdoctoral Fellowship by the Rutherford Foundation Trust and a Marsden Fast-Start Grant by the Royal Society of New Zealand.

Acknowledgements

We thank Kristy Zodrow and Peter Strege for their excellent help and Dr Nirachan Paskaranandavadivel for technical support.

Supporting Information

The following supporting information is available in the online version of this article.

Movies: Timelapse movies of emitted fluorescence *vs* time for the Fluo4 signal in the myenteric region of muscularis propria preparations from mouse small intestine. Images were collected at a rate of 1 frame every 129 ms using a 20X, 0.95 NA objective using an upright Olympus confocal FV1000 microscope with the confocal aperture fully open. For all image sets the Ca^{2+} transients were confirmed to be co-localized with Kit immunoreactivity in ICC were analyzed.

Movie S1. Ca^{2+} transients in ICC-MY from Ano1 WT mouse jejunum. Note that the peak fluorescence signals were coordinated across the whole field. Full frame dimensions were 317 × 317 μm.

Movie S2. Ca^{2+} transients in ICC-MY from Ano1 KO mouse jejunum. Note that the peak fluorescence signals were not coordinated. Full frame dimensions were 317 × 317 μm.

Movie S3. ICC-MY Ca^{2+} transients in organotypic cultures from Ano1 WT mouse jejunum treated with non-targeting shRNANT. Note that the peak fluorescence signals were coordinated across the whole field. Full frame dimensions were 159 × 159 μm.

Movie S4. ICC-MY Ca^{2+} transients in organotypic cultures from Ano1 WT mouse jejunum treated with shRNAAno1 to target down-regulation of Ano1 expression. Note that the peak fluorescence signals were not coordinated. Full frame dimensions were 159 × 159 μm.